An unusual magnetic structure in Sr_2FeO_3F and magnetic structures of K_2NiF_4-type iron(III) oxides and oxide halides, including the cobalt substituted series $Sr_2Fe_{1-x}Co_xO_3Cl$†

Andrew L. Hector,*[a] Christopher S. Knee,[b] Alexander I. MacDonald,[a] Daniel J. Price[c] and Mark T. Weller[a]

Received 21st April 2005, Accepted 1st June 2005
First published as an Advance Article on the web 16th June 2005
DOI: 10.1039/b505617a

An unusual $\boldsymbol{k} = [½\ ½\ ½]$ magnetic structure is reported in Sr_2FeO_3F at low temperature. The magnetic structures of $LaBaFeO_4$, $LaSrFeO_4$, $LaCaFeO_4$, Ca_2FeO_3Cl, Ca_2FeO_3Br, Sr_2FeO_3F, Sr_2FeO_3Cl, Sr_2FeO_3Br and solid solutions in the series $Sr_2Fe_{1-x}Co_xO_3Cl$ have been examined and only Sr_2FeO_3F exhibits this structure. The La_2CuO_4-type spin arrangement dominates in all these phases, with antiferromagnetic ordering in the *xy* planes. The $\boldsymbol{k} = [½\ ½\ ½]$ magnetic phase in Sr_2FeO_3F occurs below 100 K and requires La_2CuO_4-type stacking across the SrO layers and La_2NiO_4-type stacking across the SrF layers. It has been possible to show that this phase grows in domains which have purely La_2CuO_4-type stacking at higher temperatures. In the $Sr_2Fe_{1-x}Co_xO_3Cl$ series the La_2CuO_4-type magnetic structure in Sr_2FeO_3Cl and the La_2NiO_4-type structure in Sr_2CoO_3Cl coexist and structural and magnetic behaviour indicate phase segregation into cobalt- and iron-rich regions.

Introduction

The K_2NiF_4 structure consists of single perovskite layers separated by rocksalt layers, magnetically it is an example of a pseudo-two-dimensional square lattice. The interest in these magnetic structures is based on their importance to the understanding of properties such as superconductivity and magnetoresistance. Previous studies of the structures of the K_2NiF_4-type iron(III) oxide halides Sr_2FeO_3X (X = F, Cl, Br)[1,2] found evidence for unusual magnetic behaviour in Sr_2FeO_3F, in which a doubling of the crystallographic *c*-axis was necessary to model the magnetic structure.[1] Hence, an investigation is presented here on several iron(III) oxides ($LaAFeO_4$ where A = Ca, Sr, Ba) and oxide halides (A_2FeO_3X where A = Ca, Sr and X = Cl, Br; Sr_2FeO_3F) of this structure type using powder neutron diffraction (PND) data. The synthesis of isostructural cobalt and manganese oxide chlorides has also recently been reported, Sr_2CoO_3Cl[3] and Sr_2MnO_3Cl.[4] Subsequent neutron diffraction investigations have revealed long range antiferromagnetic order in both materials.[5,6]

Fig. 1 shows the unit cells of the materials studied. $LaAFeO_4$ have a standard K_2NiF_4-type unit cell in space group *I*4/*mmm* with the A sites statistically occupied by La and A atoms. The A_2FeO_3X materials, including Sr_2FeO_3F, have oxide/halide ordering in the rocksalt part of the structure. Oxide ions bridge the iron sites within the perovskite layers but the rocksalt layers have alternate AX and AO composition. The Fe–X bonding interaction is very weak, having a bond valence sum of 0.06–0.07 in Sr_2FeO_3X (X = F, Cl, Br), effectively resulting in the square pyramidal FeO_5 polyhedra as shown. The layers are also no longer separated by half a unit cell along *c* and the body centring is lost, the new space group is *P*4/*nmm*.[1]

Magnetic interactions between nearest neighbour iron sites in the perovskite layer are very strong, and in K_2NiF_4-type materials superexchange through O often results in antiferromagnetic coupling.[7] In the ordered state the moments can point along the *z*-axis (Ising antiferromagnetism), as found in K_2NiF_4 and Ca_2MnO_4,[8] or can be confined to the *xy* plane (*xy*-antiferromagnetism) in most cuprate oxides and La_2NiO_4.[9] The interplane coupling is typically much weaker,

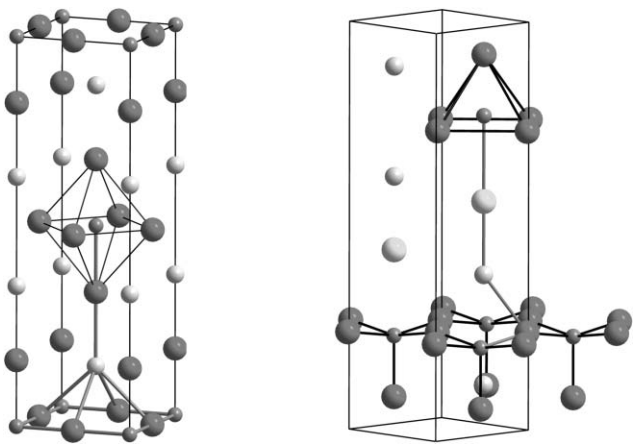

Fig. 1 Unit cells of $LaAFeO_4$ (left, *I*4/*mmm*) showing octahedral FeO_6 coordination and A_2FeO_3X (right, *P*4/*nmm*) showing square pyramidal FeO_5. Exchange pathways between iron sites in adjacent layers are shown in thick lines.

[a]*School of Chemistry, University of Southampton, Highfield, Southampton, UK SO17 1BJ. E-mail: A.L.Hector@soton.ac.uk*
[b]*Department of Applied Physics, Chalmers University of Technology and Göteborg University, SE-41296 Göteborg, Sweden*
[c]*Department of Chemistry, University of Glasgow, Joseph Black Building, University Avenue, Glasgow, UK G12 8QQ*
† Electronic supplementary information (ESI) available: powder diffraction data full collection and refinement details; representational analysis. See http://dx.doi.org/10.1039/b505617a

but nonetheless 3-dimensional (3D) ordering is often found and thus neutron diffraction becomes a useful probe of magnetic structure. Previous studies of the magnetic structures of $CaLaFeO_4$,[10] $SrLaFeO_4$[11] and our initial work on Sr_2FeO_3X materials[1] indicate *xy*-antiferromagnetic behaviour in all of the iron(III) materials.

Where K_2NiF_4-type materials exhibit 3D order, their magnetic structures are often modelled with collinear orientation of their magnetic moments. These are tetragonal structures and if all the moments are aligned along *x* or *y*, some magnetostriction should occur with a reduction in symmetry to an orthorhombic cell. Indeed, to model collinear *xy* structures a tetragonal space group cannot be used. It is usually assumed that the magnetostriction is simply too small to be observed. Fig. 1 shows one of the superexchange pathways between layers, demonstrating in $LaAFeO_4$ the equivalence of pathways between each of the iron sites in one layer of the unit cell and the iron site related to them by the body centring. This equivalence becomes very important when we consider the 3D magnetic structures since the four atoms in the bottom layer are antiferromagnetically coupled. The network of interlayer couplings is geometrically frustrated if the intralayer couplings are antiferromagnetic. In such cases it is not possible to construct a bipartite antiferromagnetic spin arrangement which satisfies all the coupling interactions. The *xy* antiferromagnetic structures only yield peaks in the PND patterns for Bragg planes with a component along *z*. Since the nuclear structures of these materials are tetragonal and no magnetostriction is resolved, the intensity of these peaks is identical for collinear and orthogonal (four sublattice) magnetic structures, *i.e.* one cannot tell whether a reflection is the 101, 011 or a combination of both. Some groups have attempted to determine experimentally whether the collinear or orthogonal structures are adopted and in these cases, the orthogonal structures have been found. One means to measure this is field dependent single crystal neutron diffraction experiments, comparing the effects of a field applied along the [100] and [110] crystallographic directions. With Nd_2CuO_4 and Sm_2CuO_4 these experiments unambiguously demonstrated the orthogonal structure and the authors of this work suggested this is likely to be adopted for the entire class of materials.[12] Collinear and orthogonal structures will yield identical results in the PND patterns, however we will use orthogonal structures in this work. It should be recognised that we do not rule out collinear models and that field dependent single crystal studies might give a different result in these Fe^{3+} systems to that found with Cu^{2+}.

Previous work on Sr_2CoO_3Cl showed that it adopts the same magnetic structure as La_2NiO_4.[5] In this work we demonstrate that Sr_2FeO_3Cl has the same magnetic structure as La_2CuO_4. In order to investigate the dependence of the magnetic structure on the transition metal, a series of samples of the nominal solid solution $Sr_2Fe_{1-x}Co_xO_3Cl$ were prepared and investigated using PND.

Experimental

$LaAFeO_4$ (A = Ca, Sr, Ba) were synthesised by the tartrate gel method previously used for $LaBaFeO_4$[13] using *ca.* 5 g $La(NO_3)_3{\cdot}xH_2O$ (Aldrich, 99.9%), $A(NO_3)_2$ (99% $Ca(NO_3)_2{\cdot}4H_2O$, $Sr(NO_3)_2$ and $Ba(NO_3)_2$, Aldrich) and $Fe(NO_3)_3{\cdot}9H_2O$ (Aldrich, 98%) in a La : A : Fe molar ratio of 1 : 1 : 1 and 2 g L-tartaric acid (99%, Aldrich). The resultant solid was pelletised and fired in air at 1350 °C for 5 hours. Powder X-ray diffraction (PXD) confirmed single phase $LaCaFeO_4$ and $LaSrFeO_4$, whereas $LaBaFeO_4$ required two more firing cycles to obtain the single phase material.

The oxide halide materials A_2FeO_3X (A = Ca, Sr; X = F, Cl, Br) were produced according to the reaction:

$$3AO + AX_2 + Fe_2O_3 \rightarrow 2A_2FeO_3X$$

Dry reagents were stored and handled in a nitrogen filled glove box. SrO and CaO were prepared from the carbonates at 1150 °C and La_2O_3 (Strem, 99.9%) was heated overnight at 1000 °C to ensure no hydroxide was present. SrF_2 (Aldrich, 99.99%), $CaBr_2$ (Aldrich, 96%), $SrCl_2{\cdot}6H_2O$ (Aldrich, 99%), $SrBr_2{\cdot}6H_2O$ (Aldrich, 99%) and Fe_2O_3 (Aldrich, 99.98%) were oven dried at 300 °C. $CaCl_2$ (Alfa Aesar, 96%) was purchased anhydrous and used as supplied. These reactions were carried out in evacuated silica tubes (lined with an alumina crucible) sealed with a torch. Reaction quantities were calculated to yield *ca.* 2 g of material, reagents were ground together thoroughly before passing down a funnel into the alumina crucible. The sealed tubes were heated at 800 °C for *ca.* 12 h and, when cool, cut open to obtain the products which were ground to brick red powders. We could not obtain Ca_2FeO_3F by this method (including variations in temperature) but did obtain A_2FeO_3X (A = Ca, Sr and X = Cl, Br) and Sr_2FeO_3F. In the case of Ca_2FeO_3Br we used a 50% excess of $CaBr_2$ as otherwise loss to volatilization led to impure products, this phase was washed with dry EtOH to remove excess $CaBr_2$ before further analysis.

The $Sr_2Fe_{1-x}Co_xO_3Cl$ series, x = 0, 0.2, 0.4, 0.6, and 0.8, were prepared through repeated reaction in air at 850 °C, with several regrinds employed in an effort to improve sample homogeneity. The reagents used were $SrCO_3$, $SrCl_2$ and Fe_2O_3, the latter two reactants were dried as described above. The brownmillerite type $Sr_2Co_2O_5$[14] precursor was used as the source of cobalt. Sample size was approximately 4 g.

PXD data were collected with graphite monochromated Cu–$K_{\alpha 1}$ radiation in Bragg–Brentano geometry with a Siemens D5000 diffractometer and PND with the OSIRIS (ISIS), D20 or D2B (ILL) diffractometers. Initial phase identification was by comparison with the PCPDF database.[15] Powder diffraction data were refined with the GSAS[16] package and full collection/refinement details are given in electronic supplementary information (ESI).†

Field cooled magnetization measurements were performed on powdered samples of Sr_2FeO_3X (X = F, Cl, Br) using a Cryogenics DC SQUID magnetometer and a Quantum Design MPMS SQUID magnetometer. Data were collected between 2 and 290 K in applied fields of 100, 200, and 2000 G. Corrections were made for the diamagnetic component of the susceptibility based on Pascal's constants.

Table 1 Refined (this work, from PXD data) and literature lattice parameters for K_2NiF_4-type iron(III) oxides and oxide halides

	a/Å	*c*/Å	Literature *a*	Literature *c*	Reference
$LaCaFeO_4$	3.8644(3)	12.3096(9)	3.867	12.300	10
$LaSrFeO_4$	3.8730(2)	12.7277(6)	3.880	12.76	11
$LaBaFeO_4$	3.9218(2)	13.1692(5)	3.921	13.175	5
Ca_2FeO_3Cl	3.83910(9)	13.6732(5)	3.848	13.65	17
Ca_2FeO_3Br	3.84398(11)	14.7750(5)	3.862	14.80	17
Sr_2FeO_3F	3.86638(4)	13.1773(2)	3.8660	13.1724	2
Sr_2FeO_3Cl	3.92042(5)	14.2966(5)	3.9239	14.2976	1
Sr_2FeO_3Br	3.93322(8)	15.1750(4)	3.9307	15.1516	1

Results

The PXD data for $LaAFeO_4$ (A = Ca, Sr, Ba) were refined to give good fits, lattice parameters matched those reported previously and are summarised in Table 1.

Previously Sr_2FeO_3F was obtained using the sealed tube method but Sr_2FeO_3Cl and Sr_2FeO_3Br were obtained by solid state reactions in air. The calcium oxide halide phases were previously grown as single crystals from CaX_2 melts.[17] The melts relied on hydrolysis from the air so it would be difficult to control the growth of a bulk sample by this method. In this work the iron oxide halides were all produced in sealed tubes due to a concern that some halide might be lost to hydrolysis when reactions are carried out in air. All five materials were obtained with good purity and the refined lattice parameters (Table 1) were a good match to literature values. The $Sr_2Fe_{1-x}Co_xO_3Cl$ series of compounds were made in air to allow direct comparison with the published[5] data on Sr_2CoO_3Cl; the Sr_2FeO_3Cl samples synthesised in a sealed tube and in air had the same cell parameters within error.

Ackerman[17] originally synthesised A_2FeO_3X (A = Ca, Sr; X = Cl, Br) as single crystals. The structures were solved in space group *P*4 with all atoms on general sites. We showed that the higher symmetry *P*4/*nmm* model used for Ba_2InO_3F[18] and Sr_2FeO_3F[2] should be used to describe Sr_2FeO_3Cl and Sr_2FeO_3Br.[1] Ackerman's structure for Ca_2FeO_3Cl has been suggested to fit this model, but without any refinements,[19] and Ca_2FeO_3Br has not been re-examined. Refinement of the structures of these two phases in *P*4/*nmm* using PXD data resulted in good fits with lattice parameters as listed in Table 1 and similar Fe–O distances to those found[1] in the Sr_2FeO_3X phases.

Magnetic structure of $LaAFeO_4$ (A = Ca, Sr, Ba)

Two basic magnetic structure types occur for 3D ordered K_2NiF_4-type *xy* antiferromagnets, those of La_2NiO_4 and La_2CuO_4.[9] These are shown in Fig. 2 and both can be described by the propagation vector $\boldsymbol{k}$ = [½ ½ 0]. The main distinction between them comes from examining the (110) planes of the nuclear unit cell (shown in dotted lines). In the La_2NiO_4 magnetic structure there is an overall ferromagnetic moment perpendicular to these planes, whereas in La_2CuO_4 there is an overall ferromagnetic moment parallel to the planes. The PND pattern of $LaCaFeO_4$ at 4 K was previously reported to yield a La_2CuO_4-type magnetic structure (modelled as collinear) with $|\mu|$ = 4.60 μ_B.[10] $LaSrFeO_4$ was found to have the La_2CuO_4 structure with $|\mu|$ = 4.23 μ_B at 4 K,[11] and this was discussed in terms of a group theory treatment and the possibility of collinear, orthogonal and intermediate structures. To our knowledge the magnetic structure of $LaBaFeO_4$ has not been previously examined. We recorded data on OSIRIS for $LaAFeO_4$ (A = Ca, Sr, Ba) at 2.4 K.

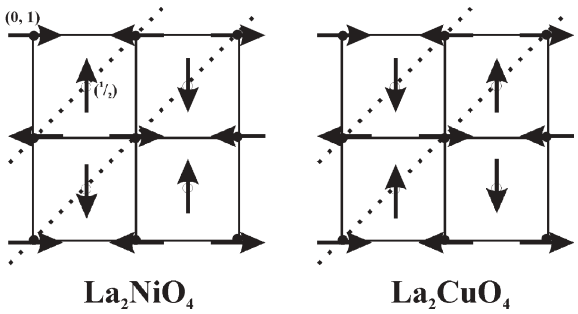

Fig. 2 Projection along *z* of K_2NiF_4-type *xy* antiferromagnetic structures. Solid lines mark the crystallographic (nuclear) unit cell, the dotted lines mark (110) Bragg planes.

The maximal non-isomorphic subgroups of order 2 describe the magnetic structures based on *I*4/*mmm*. Among these the most symmetric tetragonal space group to which we could fit the iron positions of the nuclear cell was $P4_2/nnm$ (no. 134) with a unit cell of $\sqrt{2}a \times c$ compared with the nuclear cell. The nuclear structure could be refined using the atom positions in Table 2 to a similar fit to that obtained in *I*4/*mmm* (the normal nuclear model). The 0,0,0 position used for the iron atom in $P4_2/nnm$ contains a mirror plane in (110) and the moments must therefore be 45° from the *x*- and *y*-directions. Iron also sits on a horizontal glide plane. The antiferromagnetic coupling in the *xy* plane can simply be described by these symmetry elements, completely constraining the direction of the iron moment. A diagonal glide plane defines the relationship of the magnetic moments between the layers. If the diagonal glide is normal, the La_2NiO_4 magnetic structure is obtained ($P4_2/nnm$). A time symmetric diagonal glide produces the La_2CuO_4 magnetic structure ($P4_2/nn'm$). The magnetic structures are shown in Fig. 3.

The PND data for $LaCaFeO_4$ and $LaBaFeO_4$ gave good fits to the $P4_2/nn'm$ (La_2CuO_4-type) model. The $LaSrFeO_4$ data gave a reasonable fit to this model, but underrepresented the 101 reflection and gave slightly too much intensity on the 100 and 102 reflections. However, a two-phase refinement using both the $P4_2/nn'm$ and $P4_2/nnm$ (La_2NiO_4-type) models did give a good fit, Fig. 4. Refinement using the dual phase model was carried out with all other parameters constrained to be the

Table 2 Refined nuclear and magnetic structures of $LaAFeO_4$ (A = Ca, Sr, Ba) at 2.4 K

		$LaCaFeO_4$	$LaSrFeO_4$	$LaBaFeO_4$
Magnetic space group (phase fraction in parentheses)		$P4_2/nn'm$	$P4_2/nn'm$ (0.867(6))$P4_2/nnm$ (0.133(6))	$P4_2/nn'm$
a/Å		5.47213(5)	5.47264(4)	5.54116(5)
c/Å		12.25460(20)	12.70782(14)	13.15884(21)
Fe 0,0,0 (4f)	$\mu_x = \mu_y$	3.262(15)	2.862(10)	2.872(13)
	$\lvert\mu\rvert/\mu_B$	4.614(22)	4.047(14)	4.062(19)
$La_{0.5}A_{0.5}$ 0,0,z (8m)	z	0.35568(14)	0.35578(9)	0.35677(13)
O(1) 0,0,z (8m)	z	0.17259(23)	0.16659(13)	0.16351(17)
O(2) ¼,¼,0 (4d); O(3) ¼,¾,0 (4g)				
R_{wp}, R_p (%)		5.12, 3.10	3.44, 2.31	3.57, 2.41

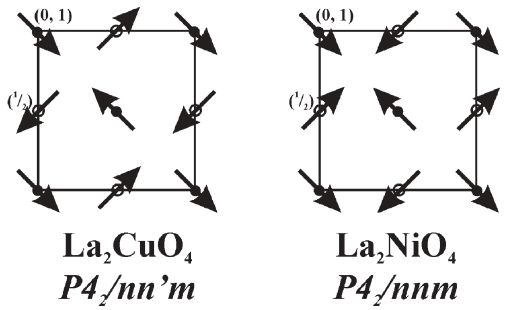

Fig. 3 Projection along z of xy antiferromagnetic unit cells of K_2NiF_4-type materials in $P4_2/nnm$.

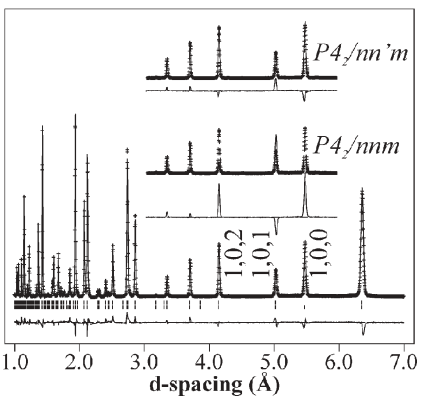

Fig. 4 Fit to the 2 K PND pattern of $LaSrFeO_4$ using a combination of $P4_2/nn'm$ and $P4_2/nnm$ magnetic structure models. Inset shows the main magnetic peaks refined using the individual models, three of which are marked with Miller indices. In the main trace, data points are marked as crosses, profile fit as the upper continuous line and difference as the lower continuous line.

same across both models. These data are summarised in Table 2.

Magnetic structures of A_2FeO_3X (A = Ca, Sr and X = Cl, Br)

Magnetic structures in this system have not previously been reported, although the 4.2 K Mössbauer spectra of Sr_2FeO_3X (X = F, Cl, Br) have been shown to be magnetically ordered.[1] The PND data (OSIRIS, 2 K) were similar to those of the oxides, extra reflections compared with the ambient temperature data were consistent with the propagation vector $\boldsymbol{k}$ = [½ ½ 0]. These included ½ ½ 0, ½ ½ 1 and ½ ½ 2 reflections of the nuclear cell and resemble the La_2CuO_4-type structures discussed above.

Table 3 Refined nuclear and magnetic structures of A_2FeO_3X (A = Ca, Sr; X = Cl, Br) at 2.4 K

	Ca_2FeO_3Cl	Ca_2FeO_3Br	Sr_2FeO_3Cl	Sr_2FeO_3Br
a/Å	5.43095(4)	5.43639(7)	5.53712(3)	5.55216(4)
c/Å	13.5895(3)	14.6877(4)	14.28269(14)	15.1421(2)
Fe ¼,¼,z (4e)	0.20648(13)	0.18905(19)	0.20716(9)	0.19513(12)
$\mu_x = \mu_y/\mu_B$	2.575(10)	2.465(20)	2.531(11)	2.686(11)
$\lvert\mu\rvert/\mu_B$	3.641(14)	3.487(28)	3.580(15)	3.799(16)
A(1) ¼,¾,z (4e)	0.0924(4)	0.0857(5)	0.09582(12)	0.09138(14)
A(2) ¼,¾,z (4e)	0.3444(4)	0.3145(4)	0.34650(15)	0.32577(15)
O(1) 0,0,z (4d)	0.2316(3)	0.2148(3)	0.23123(13)	0.21751(13)
O(2) 0,½,z (2c)	0.2316(3)	0.2148(3)	0.23123(13)	0.21751(13)
O(3) ½,0,z (2c)	0.2316(3)	0.2148(3)	0.23123(13)	0.21751(13)
O(4) ¼,¼,z (4e)	0.0681(3)	0.0620(4)	0.07478(17)	0.07079(19)
X ¼,¼,z (4e)	0.4236(2)	0.4075(3)	0.42507(10)	0.41542(15)
R_{wp}, R_p (%)	2.29, 1.71	1.49, 1.19	1.58, 1.30	1.73, 1.28

[a] Space group $P\bar{4}2_1m$.

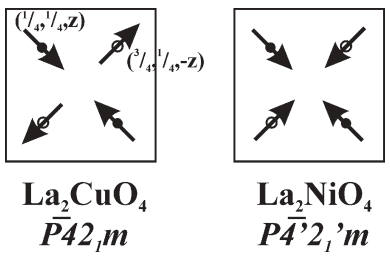

Fig. 5 Projection along z of xy antiferromagnetic unit cells of K_2NiF_4-type materials with anion ordering (*e.g.* A_2FeO_3X) in $P\bar{4}2_1m$.

The maximal non-isomorphic subgroups with order 2 of the nuclear structure space group, $P4/nmm$, were studied to see which could be used to describe the iron positions. Only in $P\bar{4}2_1m$ was this found to be possible and the atom positions in Table 3 gave a similar nuclear structure fit to the original $P4/nmm$ model. In $P\bar{4}2_1m$, the iron position at ¼,¼,z ($z \approx 0.21$) sits on a mirror plane in (110) and the direction of its moment is defined by the plane, the iron moment points into (or away from) the centre of the unit cell. If this mirror plane were time symmetric, the iron moment would be parallel to the mirror plane but the moment along z would no longer be constrained at zero. The 2-fold screw axis defines the stacking, hence $P\bar{4}2_1m$ produces a La_2CuO_4-type magnetic structure and $P\bar{4}'2_1'm$ gives a La_2NiO_4-type structure. The spin arrangements are shown in Fig. 5. As expected the $P\bar{4}2_1m$

(La_2CuO_4-type) model gave a good fit in all four cases and a full set of refined parameters is given in Table 3.

Magnetic structure of Sr_2FeO_3F

We previously found evidence for a propagation vector $\boldsymbol{k}$ = [½ ½ ½] in the magnetic reflections Sr_2FeO_3F at 2.4 K,[1] however the data were of poor resolution and no intermediate temperature data sets were recorded. An initial period of beamtime on OSIRIS showed ½ ½ ½ and ½ ½ ⅗ peaks which seemed to decay between about 2.4 K and 100 K but instrumental problems resulted in unrefinable data. A fresh sample of Sr_2FeO_3F was prepared for a second period of beamtime but the ½ ½ ½ and ½ ½ ⅗ peaks were then found to be very weak at 2.4 K. This sample was ground in a glove box and exposed to air only during packing into the sample can. Our hypothesis is that the cell doubling peaks only occur when a sample has been exposed to air, though we have not been able to test this.

The sample for the PND study on D2B and D20 was exposed to air for four weeks before use. Fig. 6 shows the variation with temperature in the magnetic reflections (D20 with 2.4 Å neutrons) of Sr_2FeO_3F. The Miller indices are labelled based on the nuclear structure. The intensity of the ½ ½ n reflections (where n = ½, ⅗, $^5/_2$ and $^7/_2$) decay as the sample temperature increases and are indistinguishable from the background at 100 K. The remaining magnetic peaks decay with temperature but are still strong at 200 K (they are also visible at ambient temperature[1]).

According to representational analysis (presented as electronic supplementary information (ESI)†), the 2 K magnetic structure of Sr_2FeO_3F must be modelled with two magnetic phases. $P\bar{4}2_1c$ is a second-order non-isomorphic subgroup of $P\bar{4}2_1m$ in which the $\boldsymbol{k}$ = [½ ½ ½] structure could be modelled. The cell doubling along c results in four layers of iron atoms rather than the two in $P\bar{4}2_1c$. The stacking arrangement between the first and second layers (also third and fourth) is controlled by the 2-fold screw axis, normally the result is a La_2NiO_4-type stacking sequence across the SrF rocksalt structured layer. A time symmetric 2-fold screw axis results in La_2CuO_4-type stacking across this layer. The diagonal glide plane defines the alignment of spins in layer three with respect to layer one (and four to two). With the iron atom at ¼,¼,z ($z \approx 0.11$) and its moment oriented perpendicular to (110), a time symmetric diagonal glide results in a structure in which La_2NiO_4- and La_2CuO_4-type stacking alternate across each rocksalt structured layer. $P\bar{4}'2_1c'$ describes the case where La_2CuO_4-type stacking is across the SrF layers and La_2NiO_4-type stacking across the SrO layers, whereas $P\bar{4}2_1'c'$ describes the reverse. The relative intensities of the 101 and 103 reflections (½ ½ ½ and ½ ½ ⅗ of the nuclear structure as shown in Fig. 6) can distinguish between these models. With our iron position and its moment perpendicular to (110), the $P\bar{4}'2_1c'$ model results in a higher intensity on 103 than on 101 whereas $P\bar{4}2_1'c'$ results in the higher intensity on 101. From Fig. 6 it is clear that the $P\bar{4}2_1'c'$ model is preferred (La_2CuO_4-type stacking across the SrO layers).

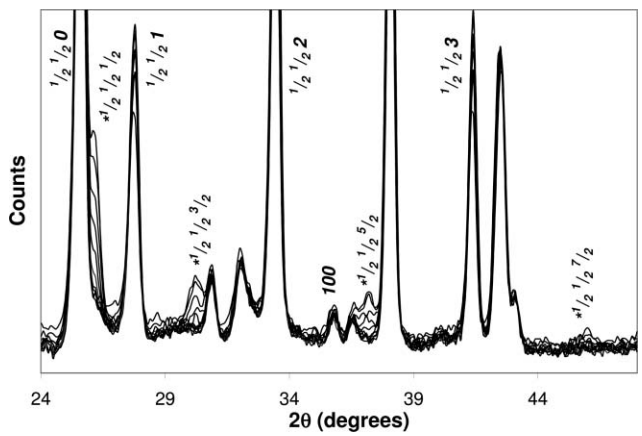

Fig. 6 Variation in the PND pattern of air-exposed Sr_2FeO_3F at 2, 10, 20, 30, 40, 50, 60, 70, 100, 150 and 200 K. Magnetic-only reflections are marked by Miller indices and peaks related to the c-axis doubling by an asterisk.

The structure was initially refined with two phases each describing the above nuclear and magnetic structures, however the peak shape on the magnetic doubled phase was found not to fit with this description. Hence we reverted to the basic $P4/nmm$ nuclear structure and refined magnetic structure as separate La_2CuO_4-type $P\bar{4}2_1m$ $\boldsymbol{k}$ = [½ ½ 0] and doubled $P\bar{4}2_1'c'$ $\boldsymbol{k}$ = [½ ½ ½] phases. Including two magnetic phases gave a reasonable fit, except that the 101 reflection of the La_2CuO_4-type phase was not intense enough and, as previously mentioned for $LaSrFeO_4$, it was necessary to include a La_2NiO_4 type component as a third magnetic phase in $P\bar{4}'2_1'm$. Some minor reflections still remained—SrF_2 was modeled as an impurity phase and reflections at 30.65°, 32.37°, 35.46° and 36.46° were excluded. One of these is attributable to the vanadium sample can, the others resemble the pattern of $LaFeO_3$ and are assumed to be a phase of $SrFeO_xF_y$ composition, though the peaks are very weak and no attempt was made to fit them.

The nuclear and magnetic structure phases were linked such that the lattice parameters and atom positions were always constant. Positions and isotropic temperature factors of all atoms in the nuclear phase were allowed to refine freely and took values consistent with the known structure.[2] With three magnetic phases it becomes impossible to jointly refine the magnetic moment on the iron atoms and all the scale factors. Since no other information about the content of each of the three magnetic phases was available, the moment was fixed and the phase fractions refined. The resultant phase fractions were then normalised such that all Sr_2FeO_3F was taken to contribute to the magnetic structure and fixed while the magnetic moment on iron was refined to give $|\mu|$ = 3.738(18) μ_B. The phase fractions, adjusted for unit cell size, were 0.816 (La_2CuO_4-type), 0.140 (doubled c-axis) and 0.042 (La_2NiO_4-type). The refined lattice parameters were a = 3.85597(2) Å and c = 13.14600(11) Å. The fit parameters were R_{wp} = 6.06% and R_P = 4.70%. The final fit to the data is shown in Fig. 7 and results from the refinement are summarised in Table 4.

As stated previously, PND data for Sr_2FeO_3F were also collected on OSIRIS. In this sample the reflections for the $\boldsymbol{k}$ = [½ ½ ½] phase were very weak, however we were able to use these data to check if a sample not exposed significantly to air still required some La_2NiO_4-type component to fit the

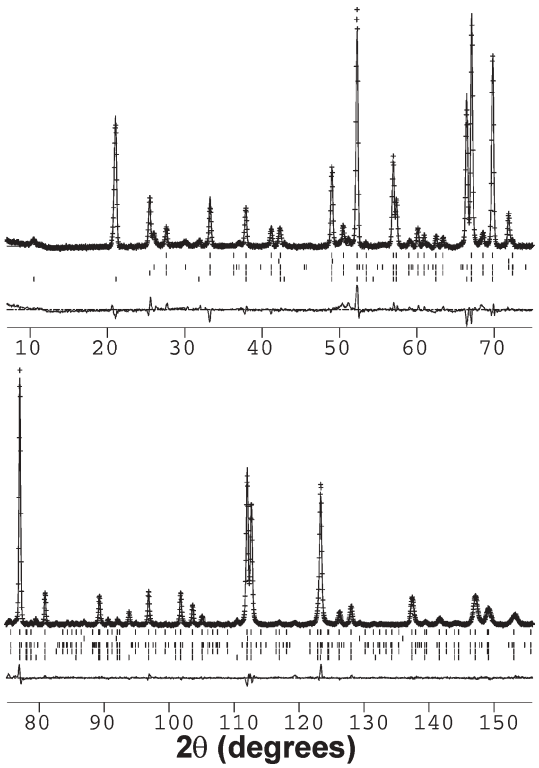

Fig. 7 Fit to the 2 K PND pattern of Sr_2FeO_3F. Allowed reflections for each phase are shown by tick marks, from bottom to top: (i) Nuclear structure of Sr_2FeO_3F in *P4/nmm*; (ii) La_2CuO_4-type magnetic structure in $P\bar{4}2_1m$; (iii) magnetic structure with $\boldsymbol{k}$ = [½ ½ ½] in $P\bar{4}'2_1c'$; (iv) SrF_2 impurity phase; and (v) La_2NiO_4-type magnetic structure in $P\bar{4}'2_1'm$. Data points are marked as crosses, profile fit as the upper continuous line and difference as the lower continuous line.

Table 4 Structure of Sr_2FeO_3F at 2 K

Nuclear structure in *P4/nmm*

a = 3.85597(2), c = 13.14600(11) Å, phase fraction = 1.00

Atom	x	y	z	$U_{iso} \times 100/Å^2$
Fe	¼	¼	0.2279(2)	0.04(5)
Sr(1)	¾	¾	0.3782(2)	0.13(7)
Sr(2)	¾	¾	0.1051(2)	0.40(8)
O(1)	¼	¼	0.0820(3)	0.70(9)
O(2)	¼	¾	0.2538(2)	0.57(6)
F	¼	¼	0.4348(3)	0.96(8)

La_2CuO_4-type magnetic structure in $P\bar{4}2_1m$

a = 5.45308(4), c = 13.14602(11) Å, phase fraction = 0.408 (0.816 if adjusted for cell size)

Atom	x	y	z	μ_x (=μ_y)/μ_B	$\lvert\mu\rvert/\mu_B$
Fe	¼	¼	0.2279(2)	2.643(18)	3.738(26)

Magnetic structure with $\boldsymbol{k}$ = [½ ½ ½] in $P\bar{4}2_1'c'$

a = 5.45309(4), c = 26.2915(5) Å, phase fraction = 0.035 (0.140 if adjusted for cell size)

Atom	x	y	z	μ_x (=μ_y)/μ_B	$\lvert\mu\rvert/\mu_B$
Fe	¼	¼	0.11397(7)	2.643(18)	3.738(26)

La_2NiO_4-type magnetic structure in $P\bar{4}'2_1'm$

a = 5.45308(4), c = 13.14602(11) Å, phase fraction = 0.021 (0.042 if adjusted for cell size)

Atom	x	y	z	μ_x (=μ_y)/μ_B	$\lvert\mu\rvert/\mu_B$
Fe	¼	¼	0.2279(2)	2.643(18)	3.738(26)

[a] R_{wp} = 6.06%, R_p = 4.70%.

magnetic structure. In this sample the phase fraction for the La_2NiO_4-type magnetic component was 0.061 when refined with the La_2CuO_4-type phase. The iron moment was refined as $|\mu|$ = 3.571(13) μ_B.

Temperature variation of the magnetic structure of Sr_2FeO_3F

PND data using the same sample as studied on D2B were collected at temperatures from 2 K to 200 K on D20. The relative intensities of the 100 and 101 reflections of the La_2CuO_4-type magnetic phase (½ ½ 0 and ½ ½ 1 in Fig. 6 based on the nuclear cell) were very similar at all temperatures studied. The La_2NiO_4-type magnetic phase content (of which the 101 reflection is most intense) was thus taken to be fairly constant. Hence a $P\bar{4}2_1m$ phase was used to model nuclear and La_2CuO_4-type magnetic phases (phase 1). A separate $P\bar{4}2_1'c'$ magnetic phase was used to model the doubled $\boldsymbol{k}$ = [½ ½ ½] contribution (phase 2). In this way it was possible to fit the important parts of the pattern with two phases, using only the high d-spacing region of the pattern.

The lattice parameters increased from a = 5.4412(3) Å, c = 13.126(2) Å at 2 K to a = 5.4481(8) Å, c = 13.135(4) Å at 200 K. Fig. 8 shows the variation in the refined magnetic moment $|\mu|$ with the refined phase fraction of phase 2 (the phase fraction of phase 1 was kept at unity). The real ratio of phase 1 : phase 2 content should be considered to be 1 : (2 × the value in the graph) because the unit cell volume of phase 2 is twice that of phase 1. It is clear from Fig. 8 that the moment on phase 1 decreases as phase 2 grows in intensity. From 100 K, the phase fraction of phase 2 refined to zero and was fixed at zero.

The magnetic susceptibility of Sr_2FeO_3X (X = F, Cl, Br) is shown in Fig. 9. This behaviour and the linear field dependent data obtained at 290 K are consistent with the assignment of antiferromagnetically ordered phases where T_N is above 300 K. It is interesting that the magnetic behaviour of the fluoride is quantitatively different from the other halides below 100 K, in the same temperature regime as the new magnetic phase grows into the PND data.

When refining magnetic moments from PND data, the obtained values are intimately correlated to the fraction of material that produces scattering and to the size of the

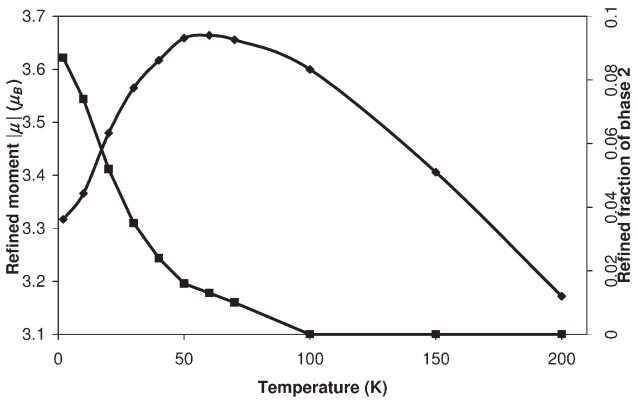

Fig. 8 Magnetic moment of iron in Sr_2FeO_3F (diamonds) and phase fraction of the $\boldsymbol{k}$ = [½ ½ ½] magnetic phase (squares).

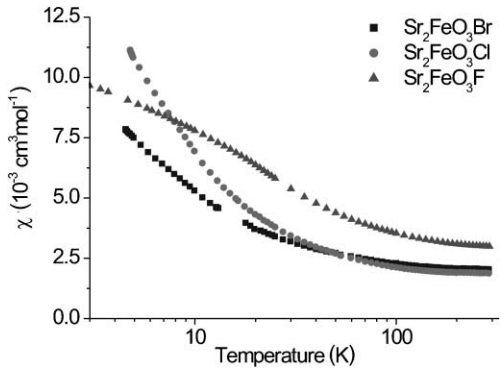

Fig. 9 Magnetic susceptibility curves of Sr_2FeO_3F, Sr_2FeO_3Cl and Sr_2FeO_3Br.

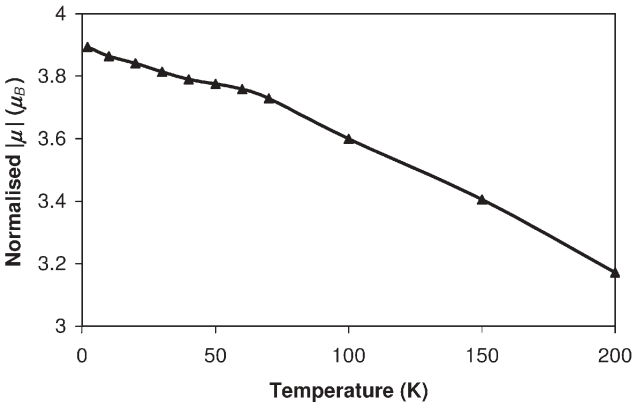

Fig. 10 Temperature variation of the iron magnetic moment in Sr_2FeO_3F normalised to total magnetic phase content.

magnetic domains; these will be difficult or impossible to deconvolute. Using the refinement method described above, the variation in the refined moment is a measure of the amount of La_2CuO_4-type magnetic scattering. This scattering falls as the phase 2 fraction, representing scattering from the doubled magnetic phase, grows. This suggests a phase change in some La_2CuO_4-type magnetic domains, rather than the presence of a separate magnetic phase with a 3D ordering temperature in the 100 K region. Normalisation of the phase fractions to reflect the real scattering levels results in the trend in $|\mu|$ shown in Fig. 10, calculated as:

$$\text{Normalised } |\mu| = \text{Refined } |\mu| \times \{\text{phase 1 fraction} + (2 \times \text{phase 2 fraction})\}$$

where the phase 1 fraction is 1.00 and the doubling of the phase 2 fraction takes into account the unit cell size. There is still an inflection in the curve at around 100 K, but the moment falls fairly smoothly with increasing temperature, supporting the argument that phase 2 grows as a result of a phase change from phase 1.

Nuclear structures of the $Sr_2Fe_{1-x}Co_xO_3Cl$ series

Rietveld analysis of the room temperature and 2 K $Sr_2Fe_{1-x}Co_xO_3Cl$ data proceeded using the *P4/nmm* symmetry to model the nuclear structure of the phases and the results are summarised in Table 5. In the final stages of the Rietveld analysis the occupancy of the mixed Fe/Co square pyramidal site was permitted to vary and in all instances refined, within error, to the targeted composition of the sample.

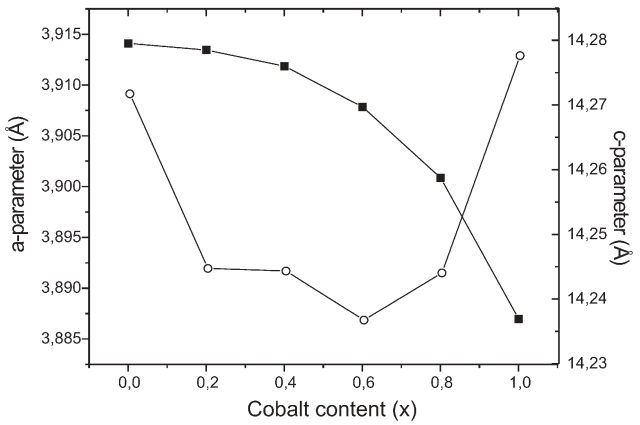

Fig. 11 Variation of the *a* (solid squares) and *c* (open circles) cell parameters with cobalt content in the $Sr_2Fe_{1-x}Co_xO_3Cl$ series. Data for the x = 1 sample is taken from reference 5.

The cell parameters of the $Sr_2Fe_{1-x}Co_xO_3Cl$ series refined from 2 K data sets are plotted in Fig. 11, also plotted are the lattice constants obtained for Sr_2CoO_3Cl at 3 K on D2B from our previous study.[6] The room temperature cell constants follow a similar trend. The *a*-parameter displays a strong positive deviation from Vegard's Law indicating that the $Sr_2Fe_{1-x}Co_xO_3Cl$ samples consist of Fe and Co rich clusters[20] and do not form a homogeneous solid solution despite several regrinds during synthesis. While clearly not linear, the general reduction in *a* obtained with increasing cobalt concentration

Table 5 Refined nuclear structures of $Sr_2Fe_{1-x}Co_xO_3Cl$ ($0 \leqslant x \leqslant 0.8$) at 2 K

	Fe	$Fe_{0.8}Co_{0.2}$	$Fe_{0.6}Co_{0.4}$	$Fe_{0.4}Co_{0.6}$	$Fe_{0.2}Co_{0.8}$
a/Å	3.91411(3)	3.91349(5)	3.91222(10)	3.90792(14)	3.9009(1)
c/Å	14.2716(2)	14.2448(3)	14.2451(5)	14.2369(7)	14.2444(5)
Fe/Co ¼,¾,*z* (2c)	0.20825(9)	0.2085(1)	0.2088(2)	0.2094(2)	0.2083(2)
Sr(1) ¼,¼,*z* (2c)	0.0960(1)	0.0980(2)	0.0973(2)	0.0986(2)	0.0981(2)
Sr(2) ¼,¼,*z* (2c)	0.3458(1)	0.3457(2)	0.3459(2)	0.3453(2)	0.3452(2)
O(1) ¾,¼,*z* (4f)	0.2313(1)	0.2314(1)	0.2304(2)	0.2300(2)	0.2300(1)
O(2) ¾,¾,*z* (2c)	0.0753(1)	0.0748(2)	0.0757(2)	0.0752(2)	0.0753(2)
Cl ¾,¾,*z* (2c)	0.4254(1)	0.42568(1)	0.4254(2)	0.4257(2)	0.4257(1)
R_{wp}, R_p (%)	5.88, 4.30	6.30, 4.45	6.25, 4.68	3.85, 2.78	4.76, 3.42

[a] Space group *P4/nmm*.

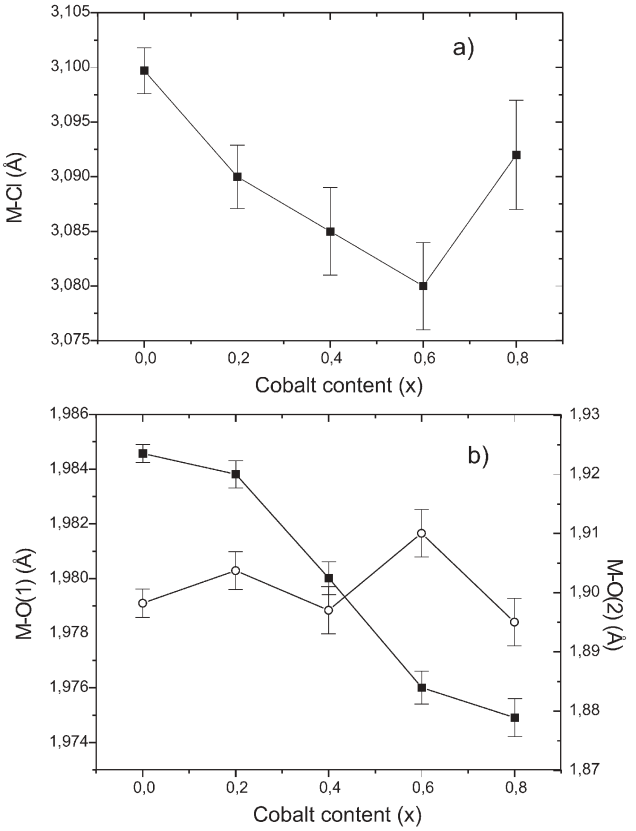

Fig. 12 Structural dependence of the $Sr_2Fe_{1-x}Co_xO_3Cl$ series: (a) shows the metal to chloride distance, (b) plots the in-plane M–O(1) bond (solid squares) and the apical M–O(2) interaction (open circles).

follows the trend expected from the ionic radii of the two ions, *e.g.* for six-fold coordination and high spin electron configurations the radii are 0.645 Å and 0.61 Å for iron(III) and cobalt(III) respectively.[21] The refined *c*-parameters settle at values significantly lower than that observed for either end members of the series and shows no clear dependence on the level of Co substitution. The origin of the contraction appears to lie with the metal to chloride distance, which shows a marked reduction for the cobalt substituted samples (Fig. 12a) indicating that increased disorder on the metal site leads to a shortened Fe/Co–Cl interaction. The average in-plane Fe(Co)–O(1) bond displays an appreciable reduction across the series reflecting the behaviour of the *a*-parameter whilst the apical M–O(2) interaction stays approximately constant at 1.900(5) Å (Fig. 12b). Finally, the planar O(1)–M–O(1) angle (not shown) remains approximately constant at $\sim$161(1)°.

Magnetic structures of the $Sr_2Fe_{1-x}Co_xO_3Cl$ series

At room temperature all samples of the $Sr_2Fe_{1-x}Co_xO_3Cl$ ($0 < x < 0.8$) series exhibited weak magnetic intensity. For the Sr_2FeO_3Cl sample low intensity reflections centred on the ½ ½ 0 and ½ ½ 2 positions were apparent above the background suggesting that the material's transition to 3D long range antiferromagnetic order occurs just above room temperature. For the samples containing cobalt the magnetic intensity consisted primarily of a broad feature spanning the

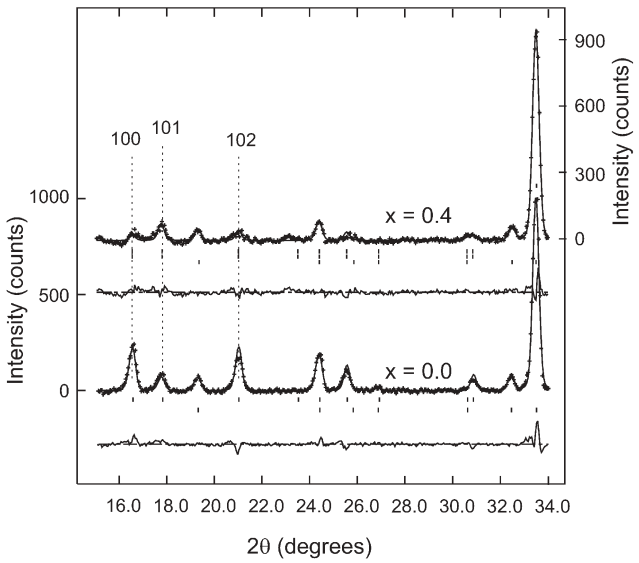

Fig. 13 Comparison of the low angle patterns obtained for Sr_2FeO_3Cl ($x = 0.0$) and $Sr_2Fe_{0.6}Co_{0.4}O_3Cl$ ($x = 0.4$) samples collected at 2 K on D2B. Crosses are observed data, lines are calculated and difference plots. Vertical tick marks indicate position of allowed reflections for the nuclear structure, lower panel, and magnetic structure(s). Also labelled are the positions of the most prominent magnetic reflections.

d-spacing range 5.5–5.1 Å, *i.e.* through the expected positions of the ½ ½ 0 and ½ ½ 1 peaks indicating a $\boldsymbol{k} = [½\ ½\ 0]$ cell.

At 2 K the magnetic intensity had resolved into more intense Bragg reflections. For the analysis of the Sr_2FeO_3Cl data the La_2CuO_4-type model developed above, space group $P\bar{4}2_1m$, was introduced as a second magnetic only phase to give a refined moment of 3.76(3) μ_B in good agreement with the value obtained of 3.58(2) μ_B determined for the Sr_2FeO_3Cl sample studied using OSIRIS. For the $x = 0.2$ sample the 100 peak (½ ½ 0 of the nuclear cell) was prominent as expected for the La_2CuO_4-type magnetic structure adopted by Sr_2FeO_3Cl. However, this reflection, which is absent for the La_2NiO_4-type magnetic lattice favoured by Sr_2CoO_3Cl, was seen to decay rapidly with increasing Co content as shown in Fig. 13. Concomitantly the intensity of the 101 reflection, the most intense line of the La_2NiO_4 magnetic structure, grew, indicating an increasing level of La_2NiO_4-type magnetic order. In order to estimate the relative amounts of the two co-existing spin structures it was assumed that the size of the Fe and Co moments in the respective magnetic domains would equal that obtained for the end members of the series, *i.e.* $|\mu| = 3.76(3)\ \mu_B$ for the Fe La_2CuO_4-type, domains and $|\mu| = 2.82(3)\ \mu_B$ for the Co La_2NiO_4-type domains.[6] The phase fractions of the two phases were then carefully refined and the results of this analysis are shown in Fig. 14. Above $x = 0.6$, the 100 reflection had become so weak that it proved impossible to reliably fit and so only the fraction of the La_2NiO_4-type cobalt phase was refined to obtain an estimate of the total coherent magnetic scattering with reference to the end members of the series.

Two main features are apparent from the analysis of the magnetic scattering obtained for the $Sr_2Fe_{1-x}Co_xO_3Cl$, $x > 0$, compounds. Firstly, the presence of a mixture of Fe and Co on

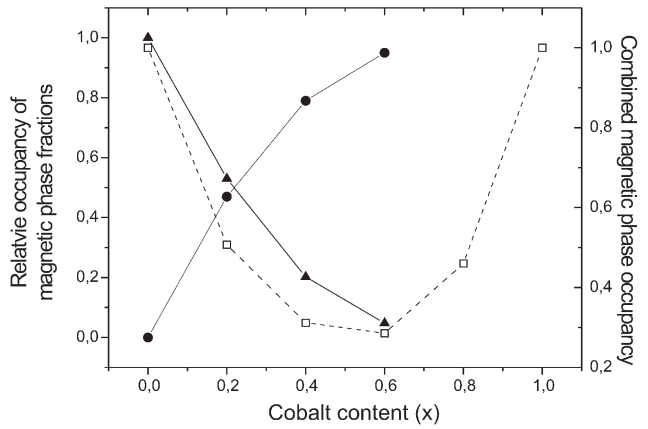

Fig. 14 Relative occupancy of La_2CuO_4 (solid triangles) and La_2NiO_4-type (solid circles) magnetically ordered domains present in the $Sr_2Fe_{1-x}Co_xO_3Cl$ compounds. Also shown (open squares) is the overall occupancy of the magnetic phases, *i.e.* the combined La_2CuO_4 and La_2NiO_4 phase fractions.

the square pyramidal sites significantly reduces the overall magnetic scattering observed. Secondly, two magnetic phases, corresponding to domains of La_2CuO_4- and La_2NiO_4-type spin order, are present. This behaviour is consistent with a phase segregation of the samples into Fe and Co rich clusters as suggested by the compositional dependence of the *a*-parameter. Furthermore, the ratio of the magnetic phase fractions (Fig. 14) does not follow a linear dependence with respect to the Fe : Co ratio as might have been expected but instead, even at low Co levels, the La_2NiO_4-type spin arrangement favoured by Sr_2CoO_3Cl is dominant. The dramatic nature of these effects is illustrated by the $x = 0.2$ sample in Fig. 14. Introduction of 20% cobalt produces a near 50 : 50 distribution of the two magnetic structures whilst the combined occupancy of the two phase fractions drops to approximately 50% of the value expected for a well ordered sample containing a single spin structure.

The large decrease in coherent magnetic intensity must be linked to increased disorder in the cobalt substituted materials. Many of the magnetically ordered domains may be too small to observe Bragg intensity and interfacial material will also not contribute to Bragg intensity. One would not expect the long range correlation within the *xy*-plane to be too severely affected by the presence of Fe–O(1)–Co linkages as the dominant interaction between is still expected to be anti-ferromagnetic if both ions are high spin.[22] As shown in Fig. 2 the only difference between the two spin lattices lies in the relative stacking of the antiferromagnetically coupled layers. It is therefore likely that the disruptive effect of mixed metal sites is most pronounced for the inter-layer coupling, *i.e.* along the *z*-direction, and in regions of the sample in which Co and Fe co-exist in similar proportions coherence in this direction is lost. The apparent robustness of the cobalt La_2NiO_4-type spin structure, even in the presence of a majority of iron spins, is somewhat harder to rationalise. At present it seems probable that the effect is related to the microstructure of the samples. For example, if it is assumed that the clusters of ordered cobalt spins are generally larger and display greater coherence than their iron counterparts, relatively more coherent magnetic scattering will be observed from the cobalt domains.

Discussion

The use of tetragonal models to describe magnetic structures in A_2MO_4 and ordered A_2MO_3X *xy* antiferromagnetic materials allows for single phase refinement of the nuclear and magnetic structures. If the magnetic domains are large (hence peak shape is the same for nuclear and magnetic components) then this simplifies refinement of these structures enormously and provides a more useful description of the magnetic symmetry.

The magnitudes of the refined moments obtained for the Fe^{3+} compounds studied here are lower than the maximum of 5 μ_B expected for high spin, d^5 systems. Similar reductions from the ideal spin-only moment are typically observed in magnetic structures refined from diffraction data due to a combination of covalency and zero point fluctuations.[23,24] In layered systems such as those investigated here it is also possible for complete ordering to be present within the antiferromagnetic sheets, whilst the inter-layer stacking is not perfectly ordered, hence we obtain low moments of the order of 3–4 μ_B even at 2 K. It is also interesting to note that in the iron materials, the oxides (Table 2) have higher moments than the oxide halides (Table 3). One might expect the better orbital overlap through chloride and bromide to increase the ordered moment with respect to those purely coupled by oxide, but this is apparently outweighed by the greater inter-layer separation.

The K_2NiF_4-type iron oxides and oxide halides all adopt the La_2CuO_4-type spin structure shown in Fig. 2, with overall antiferromagnetic coupling in the (110) planes. A minority La_2NiO_4-type phase is also observed for $LaSrFeO_4$ and Sr_2FeO_3F. The presence of this second phase in only a small number of samples implies that in the iron systems the La_2CuO_4 magnetic structure is favoured but that some small disruption, such as defects or non-stoichiometry, can stabilise the La_2NiO_4 structure in some domains.

In Sr_2FeO_3F the relative content of the La_2CuO_4 and La_2NiO_4 magnetic structure types appeared to remain fairly constant with temperature between 2 K and 200 K. This is unsurprising given that the energy difference between the interactions, which decide the stacking configurations of the layers, is likely to be very small. Recent results on the K_2NiF_4-type materials, $Sr_2CoO_2Cl_2$ and $Sr_2CoO_2Br_2$, show that they too require a mixture of the La_2CuO_4- and La_2NiO_4-type magnetic structures to fit the low temperature PND data.[25] The relative ratio of the La_2CuO_4 and La_2NiO_4-type magnetic domains present in $Sr_2CoO_2Cl_2$ remains constant below the material's T_N. In the Ising antiferromagnet Ca_2MnO_4, two magnetic phases with a similar transition temperature are observed and the authors were able to link the two spin structures to subtly different crystallographic phases.[26] We have not been able to find any literature examples of magnetic behaviour similar to that observed in Sr_2FeO_3F.

The ordered A_2FeO_3X (A = Ca, Sr; X = F, Cl or Br) phases have alternating AX and AO rocksalt layers separating the perovskite layers. Hence it is possible to see how the $\boldsymbol{k} = [½\ ½\ ½]$ magnetic structure can arise in Sr_2FeO_3F, if

La_2CuO_4-type ordering were favoured across the SrO layers and La_2NiO_4-type across the SrF layers. That this does not occur in the entire sample can also be rationalised in terms of defects or the presence of other atom types (*e.g.* oxide) in the SrF layers. This explanation does, however, require that the stacking sequence changes in the SrF layers on cooling for the growth of the $\boldsymbol{k} = [½\ ½\ ½]$ phase at the expense of the La_2CuO_4-type one. This is unusual behaviour, in the other phases presented here with a mixture of La_2CuO_4- and La_2NiO_4-type magnetic domains they appear to order together and to have a constant amount of each of theses phases. Some related behaviour has been reported by Li *et al.*[23,24] The magnetic structure of $Pb_2BaCuFeO_5Br$ can be modelled as a single magnetic phase at room temperature but a combination of several phases is necessary at 5 K.[23] Also $Y_2SrCuFeO_{6.5}$ requires two magnetic phases at 2 K, but these can also be modelled by a single phase in which the spins in one double layer are rotated by 82° to the previous double layer.[24]

The evidence that the $\boldsymbol{k} = [½\ ½\ ½]$ magnetic structure in Sr_2FeO_3F is related to the sample's exposure to air supports the link to some sort of nonstoichiometry/defects. In our previous work we presented Mössbauer data for Sr_2FeO_3F which showed that all the iron was present as Fe^{3+}, in which case the most likely cause of any deviation from the stoichiometric composition on exposure to air is the hydrolysis of some fluoride sites to hydroxide. The diffraction data give no evidence of this but only a very small number of sites would need to change in order to disrupt the balance between the weak interactions which produce the ordered stacking arrangements.

Both the OSIRIS and D2B data collected on Sr_2FeO_3Cl show the phase adopts the La_2CuO_4-type spin structure at 2 K shown in Fig. 2. The room temperature D2B data indicate that the material is barely long range ordered and the likelihood is that the transition temperature of Sr_2FeO_3Cl lies close to the T_N of 330(5) K determined for Sr_2CoO_3Cl[5] suggesting that the underlying strength of the antiferromagnetic exchange interactions in the systems is very similar. The broader point of interest as to why the isostructural phases Sr_2FeO_3Cl and Sr_2CoO_3Cl adopt different spin lattices remains an open question. In general the inter-layer interaction in such systems is believed to be at least two orders of magnitude weaker than the intra-plane coupling due to both the large separation of the ions and the primarily ionic nature of the bonds along the *z*-direction. Nonetheless, a regular stacking arrangement is crucial to 3-dimensional order and these results, as well as those previously obtained for isostructural La_2CuO_4[27] and La_2NiO_4,[28] point toward a dependence of the stacking arrangement on the transition metal. The interlayer interaction, whether associated with dipolar coulombic interactions or exchange mediated, is influenced by the transition metal. However, as shown by examples in this work, *i.e.* the biphasic magnetic scattering of the $LaSrFeO_4$ sample and the intriguing doubling of the *c*-parameter displayed by Sr_2FeO_3F, the nature of the metal ion is not the sole factor at play and further studies to understand the inter-planar interactions in these low-dimensional antiferromagnets are required.

In summary the La_2CuO_4-type magnetic structure is favoured in K_2NiF_4-type iron(III) oxides and oxide halides. In a few cases the La_2NiO_4-type magnetic structure is observed as a second minor phase and may be attributable to small variations in stoichiometry. Tetragonal structures have been developed to describe these magnetic structure types, based on the *I*4/*mmm* oxide structure and the *P*4/*nmm* oxide halide structure. Sr_2FeO_3F undergoes a magnetic phase change below 100 K, resulting in a new magnetic structure type with a four-layer stacking arrangement. The behaviour of the cobalt substituted series, $Sr_2Fe_{1-x}Co_xO_3Cl$, can be understood in terms of phase segregation into Fe and cobalt rich regions, behaviour that is reflected in both the structural and magnetic behaviour exhibited by the phases.

Acknowledgements

Thanks to Dr A. S. Wills for useful discussions and support in use of the *Sarah representational analysis* software. ALH is supported by the Royal Society through a University Research Fellowship and CSK is supported by a Marie Curie Intra-European Fellowship within the 6th European Community Framework Programme. Funding for this work was provided by EPSRC under grant GR/R99591/01. Beamtime for the neutron diffraction experiments was provided by CCLRC (RB12974, thanks to Dr K. H. Andersen for assistance with data collection) and ILL (5-31-1345, thanks to Dr T. C. Hansen for assistance with data collection).

References

1 A. L. Hector, J. A. Hutchings, R. L. Needs, M. F. Thomas and M. T. Weller, *J. Mater. Chem.*, 2001, **11**, 527.
2 G. S. Case, A. L. Hector, W. Levason, R. L. Needs, M. F. Thomas and M. T. Weller, *J. Mater. Chem.*, 1999, **9**, 2821.
3 N. Mcglothlin, D. Ho and R. J. Cava, *Mater. Res. Bull.*, 2000, **35**, 1035.
4 C. S. Knee and M. T. Weller, *Chem. Commun.*, 2002, 256.
5 C. S. Knee, D. J. Price, M. R. Lees and M.T. Weller, *Phys. Rev. B*, 2003, **68**, 174407.
6 C. S. Knee, A. A. Zhukov and M. T. Weller, *Chem. Mater.*, 2002, **14**, 4249.
7 See *e.g.* I. W. Sumarlin, J. W. Lynn, T. Chattopadhyay, S. N. Barilo, D. I. Zhigunov and J. L. Peng, *Phys. Rev. B*, 1995, **51**, 5824.
8 D. E. Cox, G. Shirane, R. J. Birgeneau and J. B. MacChesney, *Phys. Rev.*, 1969, **188**, 930; K. Tezuka, M. Inamura, Y. Hinatsu, Y. Shimojo and Y. Morii, *J. Solid State Chem.*, 1999, **145**, 705.
9 D. Petigrand, S. V. Maleyev, P. Bourges and A. S. Ivanov, *Phys. Rev. B*, 1999, **59**, 1079.
10 M. Nguyen-Trut-Dinh, M. Vlasse, M. Perrin and G. Le Flem, *J. Solid State Chem.*, 1980, **32**, 1.
11 J. L. Soubeyroux, P. Courbin, L. Fournes, D. Fruchart and G. Le Flem, *J. Solid State Chem.*, 1980, **31**, 313.
12 S. Skanthakumar, J. W. Lynn, J. L. Peng and Z. Y. Li, *Phys. Rev. B*, 1993, **47**, 6173.
13 M. Vallino, F. Abbattista, D. Mazza and A. Delunas, *Mater. Res. Bull.*, 1986, **21**, 733.
14 J. C. Grenier, S. Ghodbane, G. Demazeau, M. Pouchard and P. Hagenmuller, *Mater. Res. Bull.*, 1979, **14**, 831.
15 Powder diffraction file, International Center for Diffraction Data, Swarthmore, PA 19073, USA (version 2.4, 2004 release).
16 R. B. Von Dreele and A. C. Larson, GSAS generalised structure analysis system, Los Alamos National Laboratory, NM87545, USA (December 2002 release).
17 J. F. Ackerman, *J. Solid State Chem.*, 1991, **92**, 496.
18 R. L. Needs, M. T. Weller, U. Scheler and R. K. Harris, *J. Mater. Chem.*, 1996, **6**, 1219.
19 E. Parthé and S. Hu, *J. Solid State Chem.*, 2003, **174**, 165.

20 A. R. West, *Solid State Chemistry and its Applications*, John Wiley and Sons, 1984, pp. 367–369.
21 R. D. Shannon, *Acta Crystallogr., Sect. A*, 1976, **32**, 751.
22 J. B. Goodenough, *J. Phys. Chem. Solids*, 1958, **6**, 287.
23 R. K. Li, L. Gu and C. Greaves, *Phys. Rev. B*, 2002, **65**, 104439.
24 R. K. Li and C. Greaves, *Phys. Rev. B*, 2000, **62**, 14149.
25 C. S. Knee and M. T. Weller, *Phys. Rev. B*, 2004, **70**, 144406.
26 C. Autret, C. Martin, M. Hervieu, R. Retoux, B. Raveau, G. André and F. Bourée, *J. Solid State Chem.*, 2004, **177**, 2044.
27 D. Vaknin, S. K. Sinha, D. E. Moncton, D. C. Johnston, J. M. Newsam, C. R. Safinya and H. E. King, Jr., *Phys. Rev. Lett.*, 1987, **58**, 2802.
28 G. Aeppli and D. J. Buttrey, *Phys. Rev. Lett.*, 1988, **61**, 203.